Indian Ocean SST, Evaporation, and Precipitation during the South Asian Summer Monsoon in IPCC-AR4 Coupled Simulations

Massimo Bollasina and Sumant Nigam

Department of Atmospheric and Oceanic Science

University of Maryland, College Park, MD

Submitted to *Climate Dynamics* on June 6, 2008; revised on August 25, 2008.

Corresponding author:

Massimo Bollasina
Department of Atmospheric and Oceanic Science
3417 Computer and Space Science Building
University of Maryland, College Park, MD 20742-2425
E-mail: massimo@atmos.umd.edu

Keywords: Coupled models; South Asian monsoon; air-sea interactions; precipitation.

ABSTRACT

The veracity of modeled air-sea interactions in the Indian Ocean during the South Asian summer monsoon is examined. Representative simulations of the 20th Century climate, produced by coupled general circulation models as part of the Intergovernmental Panel on Climate Change Fourth Assessment Report, are the analysis targets along with observational data.

The analysis shows the presence of large systematic biases in coupled simulations of boreal summer precipitation, evaporation, and sea surface temperature (SST) in the Indian Ocean, often exceeding 50% of the climatological values. Many of the biases are pervasive, being common to most simulations.

The representation of air-sea interactions is also compromised. Coupled models tend to emphasize *local* forcing in the Indian Ocean as reflected by their large precipitation-SST correlations, at odds with the weak links in observations which suggest the importance of *non-local* controls. The evaporation-SST correlations are also differently represented, indicating atmospheric control on SST in some models and SST control on evaporation in others. The Indian monsoon rainfall-SST links are also misrepresented: the former is essentially uncorrelated with antecedent and contemporaneous Indian Ocean SSTs in nature, but not so in most of the simulations.

Overall, coupled models are found deficient in portraying local and non-local air-sea interactions in the Indian Ocean during boreal summer. In our opinion, current models cannot provide durable insights on regional climate feedbacks nor credible projections of regional hydroclimate variability and change, should these involve ocean-atmosphere interactions in the Indian basin.

1. Introduction

Although general circulation models (GCMs) are improving in simulating the mean global climate (e.g., Randall et al. 2007), their performance at regional scale still remains challenging. This is the case for the Asian summer monsoon. The skill of atmospheric GCMs (AGCMs) forced with observed sea surface temperatures (SSTs) in simulating the Asian summer monsoon has been fairly static (e.g., Kang et al. 2004; Wang et al. 2004), with large systematic biases still evident in the simulations (e.g., Kang et al. 2002).

Coupled atmosphere-ocean GCMs (CGCMs), too, show remarkable intra-model variability and discrepancies compared to observations (e.g., Covey et al. 2003; Meehl et al. 2005). Systematic deficiencies include a cold bias in the Pacific cold tongue and warm pool regions, a double-intertropical convergence zone (ITCZ), and a westward shift of El Niño Southern Oscillation (ENSO) variability (e.g., Covey et al. 2000; AchutaRao and Sperber 2006; Joseph and Nigam 2006).

An assessment of monsoon precipitation from the Intergovernmental Panel on Climate Change (IPCC)-participating CGCMs (Dai 2006; Annamalai et al. 2007; Kripalani et al. 2007; Lin 2007; Waliser et al. 2007) reveals the continuing challenge of simulating the seasonal and interannual variability of the Asian summer monsoon. Current models also exhibit discrepancies with respect to observed regional air-sea feedbacks (e.g., Wu et al. 2006; Lin 2007; Wu and Kirtman 2007; Wu et al. 2007). For example, interactions in the tropical Indian Ocean (IO) have varied representation in the models. This is not altogether surprising, for, despite a long investigative history, the role of the IO in regional monsoon variability remains controversial (Annamalai and Murtugudde 2004).

The impact of IO SSTs on the interannual variability of South Asian monsoon precipitation has been ascertained from both diagnostic (e.g., Rao and Goswami 1988; Harzallah and Sadourny 1997; Clark et al. 2000) and modeling (e.g., Zhu and Houghton 1996; Chandrasekhar and Kitoh 1998) studies. Overall, the relationship between IO SST and monsoon rainfall still remains poorly characterized.

Given the previous considerations, this study aims at addressing the following questions: are coupled models able to simulate the local observed atmosphere-ocean interactions in the IO during the summer monsoon? Do antecedent SSTs in the IO realistically affect summer precipitation over India in coupled models?

Systematic model biases in precipitation, evaporation, SST and near-surface winds are first analyzed since they also affect the correct representation of air-sea interactions. Secondly, *local* and *non-local* air-sea relationships are documented by computing lead-lag correlations.

The paper is organized as follows: after describing the data used in Section 2, Section 3 describes the model biases over the Indian Subcontinent. Section 4 discusses air-sea interactions, and Section 5 analyses the relationship between Indian precipitation and surrounding SSTs. Summary and conclusions follow in Section 6.

2. Model Data and Observations

Model data for the 20th Century climate integrations were collected from the World Climate Research Programme (WCRP) Coupled Model Intercomparison Project phase 3 (CMIP3). Only five representative models (all without any form of "flux adjustment")

were analyzed in this study (see Table 1) given the limited computational resources available and to avoid some redundancy of the results.

Precipitation data came from the Climate Prediction Center (CPC) Merged Analysis of Precipitation (CMAP; Xie and Arkin 1997), available on a 2.5° x 2.5° grid from January 1979 onward.

The All-India rainfall time series (AIR; Parthasarathy et al. 1995), a combination of 306 almost uniformly-distributed station measurements, was also used. Updated time series were downloaded from the website of the Indian Institute of Tropical Meteorology (http://www.tropmet.res.in).

SSTs were taken from the Hadley Centre Sea Ice and Sea Surface Temperature dataset (HadISST), which is a unique combination of global SST and sea ice concentration on a 1° x 1° grid from 1870 to date.

Evaporation data were obtained from the Woods Hole Oceanographic Institution (WHOI) Objectively Analyzed air-sea Heat Fluxes (OAFlux) dataset, an optimal blending of multi-platform satellite retrievals and numerical weather prediction reanalyses (Yu et al. 2008) available from 1958 onward on a 1° x 1° grid.

The ECMWF Reanalysis (ERA-40; Uppala et al. 2005) provided atmospheric variables on a 2.5° x 2.5° grid.

This analysis is based on 22 years (1979-1999) of monthly data, referred to also as the "climatology".

3. Seasonal Precipitation, SST, and Evaporation

a. Seasonal precipitation and 850-hPa circulation

Summertime (June-September, JJAS) precipitation and 850-hPa winds in observations and the departure of each model from observations are shown in Fig. 1. Significant large-scale biases are evident in all models: excessive precipitation over the western-central north equatorial IO and the Maritime Continent, and precipitation deficit in the south-central equatorial IO with extension into the Bay of Bengal. The meridional dipole structure of the bias suggests that the ITCZ is shifted northwestward in these models. Other notable precipitation biases include reduced rainfall along the western coast of India and excessive rain over peninsular India. The simulated 850-hPa circulation shows anomalous easterly/southeasterly winds over the western IO, consistent with excessive rainfall there. This circulation bias attenuates the prevailing cross-equatorial southwesterly flow that carries moisture to the Subcontinent.

b. Monsoon evolution

The evolution of South Asian monsoon precipitation is examined in Fig. 2 by displaying the time-latitude cross-section over the Indian sector (60º-100ºE). In observations, the rain belt moves significantly northward from ~5ºS in winter to ~15ºN in summer. An additional convergence zone exists over the eastern equatorial IO (~5ºS): it is a bit weakened during the Asian monsoon onset, but it recovers with monsoon's waning, indicating a competition between oceanic and continental convection zones.

This competition during boreal summer is largely absent in the coupled simulations, except, perhaps, in the GFDL (and ECHAM) models. The oceanic convection zone (10ºS-Equator) is not evident in the other simulations, consistent with summer precipitation underestimation in this region (cf. Fig. 1). There are other discrepancies

between observations and coupled simulations as well, relating to interrupted northward progression of the monsoon (e.g., MIROC) and delayed onset (e.g., HadCM3), for example. The monsoon evolution in the GFDL model seems reasonable but for the skewed amplitudes of the convection zones.

c. Rainfall over the Indian Subcontinent and the southern equatorial Indian Ocean

The distribution of monsoon precipitation over the South Asian continent and the IO is examined in Fig. 3a, which displays the spatial correlation between simulated and observed precipitation. Not surprisingly, correlations are highest in winter, when precipitation is confined to smaller regions. The correlations decrease with the arrival of monsoon rains, principally from differences in the distribution over the IO. MIROC and CCSM3 stand out as particularly deficient, using this metric.

The annual cycle of precipitation averaged over two key monsoon regions (India and the southern IO) is depicted in Figs. 3b and 3c, respectively. Only land point values were included in the average over India, given our intent to compare simulations against station-based rainfall climatology (AIR) as well. Oceanic precipitation was averaged over the region exhibiting strong negative bias in Fig. 1. That CMAP and AIR estimates are indistinguishable in Fig. 3a is reassuring. The average rainfall over the Subcontinent is simulated quite reasonably, although differences in the timing of the peak and duration of the rainy season are recognizable (e.g., a delayed monsoon onset in HadCM3, a too gradual and anticipated onset in CCSM3, a weaker peak rainfall and prolonged rainy season in GFDL). In contrast, modeled rainfall over the south-central IO shows great

variance with respect to observations, and even among simulations. As noted earlier, only the GFDL model produces realistic seasonal variation of rainfall in this region.

d. Seasonal SST variability in the coupled simulations

The seasonal variability of SST in the coupled simulations is examined in Fig. 4, which shows the amplitude and phase of the annual cycle using vectors. The annual-mean SSTs are contoured for reference. The warmest SSTs are observed in boreal spring when the 29ºC contour encloses the area from 10ºS to 15ºN. The monsoon onset leads to cooling of SSTs in the northern IO, especially along the Somali coast. In the northern Arabian Sea and the Bay of Bengal, SSTs are warmest a few months later, in mid summer.

The CGCMs can generate fairly realistic annual-mean SST distributions, as seen in Fig. 4. HadCM3 produces the warmest SSTs, especially in the 5ºS-5ºN belt, with the western IO warmer by ~1.5ºC. The GFDL and MIROC models, on the other hand, produce a slightly cold equatorial region. The SST annual cycle in the southern Tropics is realistically captured in all simulations, but the corresponding variability in the western and northern IO is challenging for the models, especially CCSM3 and HadCM3. CCSM3, HadCM3, and MIROC have also a weak seasonality along the Equator.

e. Monsoon season SST and near-surface winds

SSTs and near-surface winds in the monsoon season are displayed in Fig. 5. Model departures from observations are shown, as in Fig. 1. The simulation of SST is apparently challenging, especially along the Somali Coast and the south-central IO, i.e., in the regions of notable precipitation error (cf. Fig. 1). A cold bias also surrounds the Indian

peninsula in many simulations. The SST bias defies further characterization. The near-surface winds have a southeasterly component across much of the IO. The bias is similar to that of the 850-hPa wind (cf. Fig. 1), but not in all simulations (e.g., MIROC). The biased wind is often directed from the cold SST-bias regions into the warm ones.

As a result, the speed of the trade winds in the Southern Hemisphere (SH; see also Fig. 6) is increased but the Somali Jet is damped, affecting local SSTs (through increased ventilation and reduced coastal upwelling, respectively). The southeasterly bias also opposes the monsoon westerlies north of the equator, leading to reduced wind speed and evaporation there, which are reflected in the region's warm SST bias.

f. Evaporation biases in coupled simulations

The potential of coupled GCMs in simulating summertime evaporation over the IO is examined in Fig. 6, where evaporation biases are superposed on wind-speed biases. As before, the observed full fields are shown in the top-left panel. In nature, evaporation is largest near the Tropic of Capricorn, both from wind speed effects but even more because of humidity differences arising from the fluxing of dry air off the northern flank of the robust Mascarene High in the SH winter. Wind speeds are again large in the Arabian Sea, but not evaporation as the air is already quite saturated at this point in its journey towards the Continent. The upwelling colder SSTs extending off the Somali Coast are not helpful either.

Evaporation in the coupled simulations is not as tightly centered around the Tropic of Capricorn as in observations, since it extends northward up to the equator, especially in the western IO. The northward extension is not all due to the bias in wind speed, which is

focused further to the north, since other factors can contribute in determining evaporation (e.g., near-surface vertical humidity gradients). The wind bias is connected to an anomalous vertical circulation, which manifests in the pattern of the regional upper-tropospheric divergent circulation.

g. Divergent circulation biases in coupled models

The performance of CGCMs over the South Asian sector is placed in global context in Fig. 7 which shows the divergent circulation at 200 hPa, the level of monsoonal outflow. As before, model biases with respect to observations (ERA-40) are displayed. Comparison of CMAP rainfall (Fig. 1) and ERA-40 divergent circulation shows excellent qualitative agreement between regions of strong precipitation (i.e., strong latent heat release) and upper-tropospheric divergence in the Tropics/subtropics. The strongest upper-level divergent flow originates in the Bay of Bengal and heads northwestward (e.g., Rodwell and Hoskins 2001), westward, and southward. The southward component converges over the southern subtropical IO, strengthening the Mascarene High (Krishnamurti and Bhalme 1976; Nigam and Chan 2008). The divergence bias in the coupled simulations is consistent with the precipitation bias in the IO, especially in the GFDL and MIROC models. The analysis, unfortunately, did not provide insights into the cause of the biases in the IO. Notable biases are not confined to the IO basin alone, since equally impressive differences are present over the Maritime Continent and the Pacific ITCZ. This pattern suggests that the ITCZ and its SH counterpart are displaced in coupled simulations, often due to the existence of a double-ITCZ (e.g., Lin 2007).

h. Atmospheric water balance over the southern Indian Ocean

The JJAS atmospheric water-balance over the southern equatorial IO is examined in Fig. 8 to gain insight into the cause of the simulated precipitation deficit. The three-leading budget terms – evaporation (E), precipitation (P), and column moisture flux convergence (MFC) – are displayed. The column moisture tendency (typically, small; ~0.1 mm day^{-1}) is not shown, and MFC does not include the transient flux contribution as sub-monthly data was unavailable for the simulations. If ERA-40 estimate of the transient MFC over the IO (~0.6 mm/ day^{-1}) is of guidance, the non-inclusion of the transient contribution is not a serious omission.

It is noteworthy that the observational budget itself is somewhat uncertain. The water balance is constructed from ERA-40 stationary MFC, CMAP precipitation, and OAFLUX evaporation. The imbalance or residue (RES = P−E−MFC) is also plotted in Fig. 8. ERA-40 precipitation and evaporation fields are not used because reanalysis procedures are generally not mindful of the atmospheric or terrestrial water-balance (Nigam and Ruiz-Barradas 2006).

Over the ocean, CCSM3, HadCM3 and MIROC show E−P to be positive (and MFC of opposite sign than observations), while the opposite is true for GFDL and ECHAM (in line with observations). Despite such variation, the model budgets are balanced, attesting to the smallness of column moisture tendency and transient MFC. The negative MFC over the southern equatorial IO in the simulations exhibiting the largest precipitation

biases suggest that the latter is due to the presence of divergent circulation in the lower troposphere rather than any diminished availability of moisture.

4. Local air-sea feedbacks in the Indian Ocean

Local contemporaneous correlations among P, E, and SST are examined in this section with the purpose of investigating atmosphere-ocean feedbacks in the IO during the summer monsoon. All correlations are computed on monthly anomalies, after subtracting the monthly climatological annual cycle. Given the length of the time series (1979-1999), the 90%, 95%, and 99% confidence levels are at 0.21, 0.24, and 0.31, respectively.

As the atmosphere responds rapidly to SST, a large positive simultaneous correlation of P and SST indicates SST's influence on the atmosphere. On the other hand, a large negative correlation between P and SST-tendency is suggestive of atmosphere's influence on SST (e.g., Wu and Kirtman 2005). The observed summer correlations shown in the top panels of Fig. 9a indicate generally weak links between P, E, and SST.

The P-SST correlation is weakly positive except in the eastern equatorial IO (85°-100°E, 10°S-5°N), where it is moderately large. Precipitation and SST-tendency (not shown) are positively and weakly correlated here. This suggests that SST strongly forces the atmosphere over the eastern IO, which, in turn, has a positive feedback on SSTs. A weaker SST influence on the atmosphere is found over the western equatorial and sub-equatorial IO, associated with a very weak negative precipitation-SST tendency correlation (denoting a weak negative atmospheric feedback). Over the northern IO, a negligible positive P-SST correlation associated with a significantly negative P-SST

tendency correlation suggests that the atmosphere can exert control on SST here. Our finding that SST variability is influential in a very limited region of the IO is consistent with the lead-lag correlation analysis of Wu and Kirtman (2007).

Inspection of Figs. 9a-b shows that the simulated P-SST link is too strong in the equatorial IO, especially for three models (CCSM3, HadCM3, and MIROC). Wu et al. (2006) reported similar findings for the COLA coupled model. The P-SST correlation structure in the GFDL simulation, on the other hand, is reasonably realistic, although values are overestimated. The simulated precipitation-SST tendency correlation (not shown) is negative and quite large in the north equatorial and in the western IO, while it is positive in the eastern south equatorial IO. These patterns indicate that coupled models are characterized by an excessive oceanic forcing on the atmosphere over the equatorial IO with mostly negative feedback except over the eastern IO, and by a too strong impact of atmospheric anomalies on the SST in the northern IO.

The second observational panel shows the variations of E and SST to be weakly and positively correlated. Significant values are found in the upwelling region off the Somali coast, reflecting the SST influence rather than the wind-speed effect.[1] The GFDL and ECHAM models have E and SST positively correlated (as in observations), but much too strongly. The other three models exhibit a band of negative E-SST correlations in the equatorial IO sector, reflecting the wind-speed influence (or atmospheric control) on E. Wu et al. (2006) have also investigated the E-SST linkage but for the whole year rather than just the monsoon season, as here. The observed evaporation-SST tendency correlation (not shown) is negative over the larger part of the domain, suggesting the

[1] Stronger wind speeds would be associated with a stronger Somali jet, and thus colder upwelled SSTs. Dominance of the wind-speed effect in this region would manifest as a negative E-SST correlation.

predominant contribution of evaporation to SST anomalies (in agreement with the small values of the evaporation-SST correlation). Values are slightly positive in the northern IO north of 10°N and over the western IO, where the evaporation/SST correlations are positive and larger. All models show strong negative correlations over most of the IO and much larger than observations, indicating a too strong atmospheric forcing on SST.

The third observational panel (Fig. 9a) shows the P and E variations to be essentially uncorrelated, indicating that the variability of precipitation is only partially modulated by local variations of moisture through evaporation, and that other processes (i.e., large-scale dynamics) play an important role. This is clearly not the case for the coupled simulations, though. All models, and CCSM3 in particular, show large negative P-E correlations from the Maritime Continent across the equatorial IO, indicating a too strong forcing of the atmosphere on surface evaporation.

5. Indian summer monsoon and Indian Ocean SSTs

The non-local influence of IO SSTs on precipitation over India is analyzed in this section. The antecedent and simultaneous correlations of Indian summer monsoon rainfall with surrounding SSTs are shown in Fig. 10. Correlations are shown for SSTs leading by 6 months, 3 months, and 0 months, and for SSTs lagging by 3 months (i.e., with previous December-February (DJF), March-May (MAM), simultaneous SSTs, and following September-November (SON), respectively). The Indian summer monsoon is, evidently, weakly linked to IO SSTs. Only previous winter's SST in the southeastern IO and the northern Arabian Sea appears to be marginally influential, consistently with

findings of Clark et al. (2000). Interestingly, in the autumn following the monsoon, the correlations become significantly negative in the northern IO.

The linkage between all-India precipitation and surrounding SSTs is variedly represented in the coupled simulations, with the GFDL and ECHAM models showing significant negative correlations and CCSM3 modestly positive ones at all lags. In both cases, correlations are at variance with observations. Interestingly, HadCM3, which contains significant seasonal biases in IO precipitation and SST (cf. Figs. 1 and 5), appears more realistic from the viewpoint of Indian summer monsoon-SST links. In contrast, the GFDL and ECHAM simulations, deemed most realistic from the local correlation analysis perspective, contain significant negative correlations in the western IO, especially at zero lag, where observed values are close to zero.

It is, of course, not difficult to envision excessive Indian monsoon rainfall as being due to stronger monsoonal flow over the western IO (and along the Somali Coast). The stronger flow would generate more evaporation and coastal upwelling, both responsible for cooling SSTs (e.g., Meehl et al. 2006). This link is supported by observations but only during the post-monsoon fall. Recently, Kulkarni et al. (2007) has also noted the influence of the Indian monsoon on fall SSTs over the Indian Ocean. Local simultaneous correlations, moreover, show E and SST to be positively correlated along the Somali coast in observations (Fig. 9a), indicating SST control on E in the region and not vice-versa.

6. Summary and Conclusion

This study examines the veracity of modeled air-sea interactions in the IO basin during the South Asian summer monsoon. Representative coupled models simulations of the 20th Century climate, produced for the IPCC-AR4, are the analysis targets along with observations.

The examination is motivated by the need to assess the realism of climate variability mechanisms operating in the South Asian sector in coupled models. These models are being increasingly used to forecast changes in *regional* hydroclimate in response to rising greenhouse gas concentrations and aerosol loadings, but without sufficient acknowledgement of the model shortcomings, especially on regional scales. The perceived overreliance on models in investigations of aerosols influence on South Asian hydroclimate (e.g., Menon et al. 2002; Lau et al. 2006; Chung and Ramanathan 2006; and recently Meehl at al. 2008) instigated this analysis.

The seasonal variability of precipitation, evaporation, SST, near-surface winds, and moisture fluxes over the Indian Subcontinent and the IO for the period 1979-1999 was analyzed. Related published studies of Dai (2006) and Lin (2007) provided context for this analysis, which is focused on boreal summer.

Our analysis shows the presence of large systematic biases in the simulated precipitation, evaporation, and SST over the IO, often exceeding 50% of the climatological values. Many of the biases are pervasive, being common to all models.

Coupled simulations are found compromised also in representation of atmosphere-ocean interactions. Models (e.g., CCSM3, HadCM3, and MIROC) tend to strongly overestimate local air-sea coupling in the Indian basin, as reflected by their large

precipitation-SST correlations at variance with the insignificant observed values. The evaporation-SST correlations are also differently represented, with the above three simulations exhibiting modest negative values (or atmospheric control) while the other two (i.e., GFDL and ECHAM) strongly positive ones (or SST control) in the equatorial IO, at odds with the modest positive correlations in observations.

Our analysis suggests that CCSM3's behavior, for example, can be best described as being *local* over the equatorial IO, with larger SSTs leading to more precipitation. On the contrary, evaporation is erroneously controlled by the atmosphere in this model. In nature (and to an extent in the GFDL and ECHAM models), *local* SSTs are not influential on precipitation, indicating the importance of *non-local* controls.

The relationship between SST and Indian summer monsoon rainfall also shows a distorted representation of ocean-atmosphere interactions in the coupled simulations. Indian monsoon rainfall is essentially uncorrelated or weakly correlated with both antecedent and contemporaneous IO SSTs in observations, but not so in models, especially GFDL and ECHAM.

At this stage this analysis provides rather limited insight on the cause of the models aberrant behavior. Given the myriad of dynamical and thermodynamical coupled physical processes in play in the IO during boreal summer, determining the reasons of model biases can be a challenging and arduous task. Local and non-local air-sea interactions can be differently simulated by models. For example, one is at a loss in explaining why models with distorted local air-sea interaction (e.g., HadCM3) do better in representing the non-local relationships (cf. Fig. 10). Answering such questions will require controlled model experimentation, which is beyond the scope of the present study.

We find that several coupled climate models used in the IPCC-AR4 are seriously deficient in their portrayal of air-sea interactions in the IO during boreal summer. In our opinion, they cannot provide durable insights on regional climate feedbacks nor credible projections of regional hydroclimate variability and change, should these involve ocean-atmosphere interaction in the IO.

Acknowledgements

The authors acknowledge NOAA and NSF support through CPPA-NA17EC1483 and ATM-0649666 grants.

References

AchutaRao KM, Sperber KR (2006) ENSO Simulation in Coupled Ocean-Atmosphere Models: Are the Current Models Better?. Clim Dyn 27: 1-15

Annamalai H, Hamilton K, Sperber KR (2007) South Asian Summer Monsoon and its relationship with ENSO in the IPCC AR4 simulations. J Climate 20: 1071-1092

Annamalai H, Murtugudde R (2004) Role of the Indian Ocean in regional climate variability. In Earth's Climate: The Ocean-Atmosphere Interaction. Geophys Monograph Series 147: 213-246

Chandrasekar A, Kitoh A (1998) Impact of localized sea surface temperature anomalies over the equatorial Indian Ocean on the Indian summer monsoon. J Meteor Soc Japan 76: 841–853

Chung CE, Ramanathan V (2006) Weakening of North Indian SST gradients and the monsoon rainfall in India and the Sahel. J Climate 19: 2036-2045

Clark CO, Cole JE, Webster PJ (2000) Indian Ocean SST and Indian summer rainfall: predictive relationships and their decadal variability. J Climate 13: 2503-2519

Covey C, AchutaRao KM, Cubasch U, Jones P, Lambert SJ, Mann ME, Phillips TJ, Taylor KE (2003) An Overview of Results from the Coupled Model Intercomparison Project (CMIP). Global Planet Change 37: 103-133

Covey C, AchutaRao KM, Lambert SJ, Taylor KE (2000) Intercomparison of Present and Future Climates Simulated by Coupled Ocean-Atmosphere GCMs. PCMDI Report No 66. Program for Climate Model Diagnosis and Intercomparison, Lawrence Livermore National Laboratory, University of California, Livermore, CA

Dai A (2006) Precipitation characteristics in eighteen Coupled Climate Models. J Climate 19: 4605-4630

Harzallah R, Sadourny R (1997) Observed lead-lag relationships between Indian summer monsoon and some meteorological variables. Clim Dyn 13: 635–648

Joseph R, Nigam S (2006) ENSO evolution and teleconnections in IPCC's Twentieth-Century climate simulations: realistic representation? J Climate 19: 4360–4377

Kang IS, Lee JY, Park CK (2004) Potential predictability of summer mean precipitation in a dynamical seasonal prediction system with systematic error correction. J Climate 17: 834-844

Kang IS, and Coauthors (2002) Intercomparison of the climatological variations of Asian summer monsoon precipitation simulated by 10 GCMs. Clim Dyn 19: 383-395

Kulkarni A, Sabade SS, Kripalani RH (2007) Association between the extreme monsoons and the dipole mode over the Indian subcontinent. Meteorol Atmos Phys 95: 255-268

Kripalani RH, Oh JH, Kulkarni A, Sabade SS, Chaudhari HS (2007) South Asian summer monsoon precipitation variability: Coupled climate model simulations and projections under IPCC AR4. Theor Appl Climatol 90: 133-159

Krishnamurti TN, Bhalme HN (1976) Oscillations of a monsoon system. Part I. Observational aspect. J Atmos Sci 33: 1937-1954

Lau, KM, Kim MK, Kim KM (2006) Aerosol induced anomalies in the Asian summer monsoon- the role of the Tibetan Plateau. Clim Dyn 26: 855-864 doi:10.1007/s00382-006-0114-z

Lin JL (2007) The double-ITCZ problem in IPCC AR4 coupled GCMs: ocean-atmosphere feedback analysis. J Climate 20: 4497-4525

Meehl GA, Arblaster JM, Collins WD (2008) Effects of black carbon aerosols on the Indian monsoon. J Climate 21: 2869–2882

Meehl GA, Covey C, McAvaney B, Latif M, Stouffer RJ (2005) Overview of the Coupled Model Intercomparison Project. Bull Amer Met Soc 86: 89-93

Meehl GA, Arblaster JM, Lawrence DM, Seth A, Schneider EK, Kirtman BP, Min D (2006) Monsoon Regimes in the CCSM3. J Climate 19: 2482-2495

Menon S, Hansen J, Nazarenko L, Luo Y (2002) Climate effects of black carbon aerosols in China and India. Science 297: 2250-2253

Nigam S, Chan S (2008) On the summertime strengthening of the Northern Hemisphere sea-level pressure anticyclone. (in press for the J Climate)

Nigam S, Ruiz-Barradas A (2006) Seasonal hydroclimate variability over North America in global and regional reanalyses and AMIP simulations: varied representation. J Climate 19: 815-837

Parthasarathy B, Munot AA, Kothawale DR (1995) All India monthly and seasonal rainfall series: 1871-1993. Theor and Appl Climatol 49: 217-224

Randall DA, Wood RA, Bony S, Colman R, Fichefet T, Fyfe J, Kattsov V, Pitman A, Shukla J, Srinivasan J, Stouffer RJ, Sumi A, Taylor KE (2007) Climate Models and Their Evaluation. In: Climate Change 2007: The Physical Science Basis. Contribution of Working Group I to the Fourth Assessment Report of the Intergovernmental Panel on Climate Change [Solomon S, Qin D, Manning M, Chen Z, Marquis MC, Averyt KB, Tignor M, Miller HL (eds.)]. Cambridge University Press, Cambridge, United Kingdom and New York, NY, USA, 996 pp

Rao KG, Goswami BN (1988) Interannual variations in sea surface temperature of the Arabian sea and the Indian monsoon: A new perspective. Mon Wea Rev 116: 558-568

Rodwell MJ., Hoskins BJ (2001) Subtropical anticyclones and summer monsoons. J Climate 14: 3192-3211

Uppala SM, and Coauthors (2005) The ERA40 reanalysis. Q J Royal Met Soc 131: 2961-3012

Waliser D, Seo KW, Schubert S, Njoku E (2007) Global water cycle agreement in the climate models assessed in the IPCC AR4. Geophys Res Lett 34: L16705, doi: 10.1029/2007GL030675

Wang B, Kang IS, Li JY (2004) Ensemble simulation of Asian-Australian monsoon variability by 11 AGCMs. J Climate 17: 803-818

Wu R, Kirtman BP (2007) Regimes of seasonal air-sea interaction and implications for performance of forced simulations. Clim Dyn 29: 393-410

Wu R, Kirtman BP (2005) Roles of Indian and Pacific Ocean air-sea coupling in tropical atmospheric variability. Clim Dyn 25: 155-170

Wu R, Kirtman BP, Pegion K (2007) Surface latent heat flux and its relationship with sea surface temperature in the National Centers for Environmental Prediction Climate Forecast System simulations and retrospective forecasts. Geophys Res Lett 34: L17712, doi:10.1029/2007GL030751

Wu R, Kirtman BP, and Pegion K (2006) Local air-sea relationship in observations and model simulations. J Climate 19: 4914-4932

Xie P, Arkin PA (1997) Global precipitation: A 17-year monthly analysis based on gauge observations, satellite estimates, and numerical model outputs. Bull Amer Meteor Soc 78: 2539-2558

Yu L, Jin X, Weller RA (2008) Multidecade Global Flux Datasets from the Objectively Analyzed Air-sea Fluxes (OAFlux) Project: Latent and sensible heat fluxes, ocean evaporation, and related surface meteorological variables. Woods Hole Oceanographic Institution, OAFlux Project Technical Report. OA-2008-01, 64pp., Woods Hole. Massachusetts

Zhu Y, Houghton DD (1996) The impact of Indian Ocean SST on the large-scale Asian summer monsoon and the hydrological cycle. Int J Climatol 16: 617-632

Figure Captions

Figure 1: Seasonal mean (Jun-Sep; JJAS) precipitation (mm day^{-1}) and 850-hPa winds (m s^{-1}) for observations (top left) and differences model-observations (other panels).

Figure 2: Time-latitude evolution of precipitation (mm day^{-1}) averaged over (60°-100°E; land and ocean points) for observations (top left) and coupled models (other panels).

Figure 3: Annual cycle of (a) spatial correlation of model precipitation (averaged over 60°-100°E; 10°S-30°N; land and ocean points) with respect to CMAP, (b) observed and simulated precipitation (mm day^{-1}) averaged over India (land-only points), (c) observed and simulated precipitation (mm day^{-1}) averaged over (60°-100°E; 10°S-Equator) (ocean-only points).

Figure 4: Annual mean SST (ºC, shaded) and amplitude and phase (arrows) of the annual cycle of SST over the Indian Ocean for observations (top left) and coupled models (other panels).

Figure 5: Seasonal mean (Jun-Sep; JJAS) SST (°C) and 1000-hPa winds (m s^{-1}) over the Indian Ocean for observations (top left) and differences model-observations (other panels).

Figure 6: Seasonal mean (Jun-Sep; JJAS) evaporation (mm day^{-1}, shaded) and 1000-hPa wind speed (m s^{-1}, contours) over the Indian Ocean for observations (top left) and differences model-observations (other panels).

Figure 7: June-August mean (JJA) divergent wind (arrows) and divergence (10^{-6} s^{-1}; shaded) at 200 hPa in ERA40 (top) and differences model-ERA40 (other panels).

Figure 8: Seasonal (Jun-Sep) mean atmospheric water budget (in mm day^{-1}; P = precipitation; E = evaporation; MFC = vertically-integrated moisture flux convergence) averaged over (60°-100°E, 10°S-Equator).

Figure 9a: June-August average pointwise and simultaneous correlations between precipitation and SST (left column), evaporation and SST (middle column), and precipitation and evaporation (right column) for observations (top), CCSM3 (middle), and GFDL (bottom). The zero-correlation contour is also displayed.

Figure 9b: The same as Fig. 9a, except for HadCM3 (top), MIROC (middle), and ECHAM (bottom).

Figure 10a: Correlations (contour lines) and regressions (ºC; shaded) between Jun-Aug (JJA) precipitation over India and surrounding SST at (from top to bottom) lag -6, -3, 0, and +3 months (that is, SST of the previous DJF, MAM, contemporaneous JJA, and

following SON, respectively) for observations (left), CCSM3 (middle), and GFDL (right).

Figure 10b: The same as Fig. 10a, except for HadCM3 (left), MIROC (middle), and ECHAM (right).

Table 1. Climate models analyzed in this work.

Modeling Group	Model Name	AGCM resolution	OGCM resolution	Reference
National Center for Atmospheric Research	CCSM3	1.4°x1.4° L26	384x320L40	Collins et al. (2006)
Hadley Centre for Climate Prediction and Research/Met Office	HadCM3	2.75°x3.75° L18	1.25°x1.25° L20	Jones et al. (2004)
Geophysical Fluid Dynamics Laboratory	GFDL-CM2.1	2.0°x2.5° L24	1.0°x0.33° L50	Delworth et al. (2006)
Center for Climate System Research/National Institute for Environmental Studies/Frontier Research Center for Global Change	MIROC3.2	1.125°x1.125° L56	0.1875°x0.28125° L47	Hasumi et al. (2004)
Max Planck Institute for Meteorology	ECHAM5/MPI-OM	2.0°x2.5° L31	1.5°x1.5° L40	Roeckner at al. (2003)

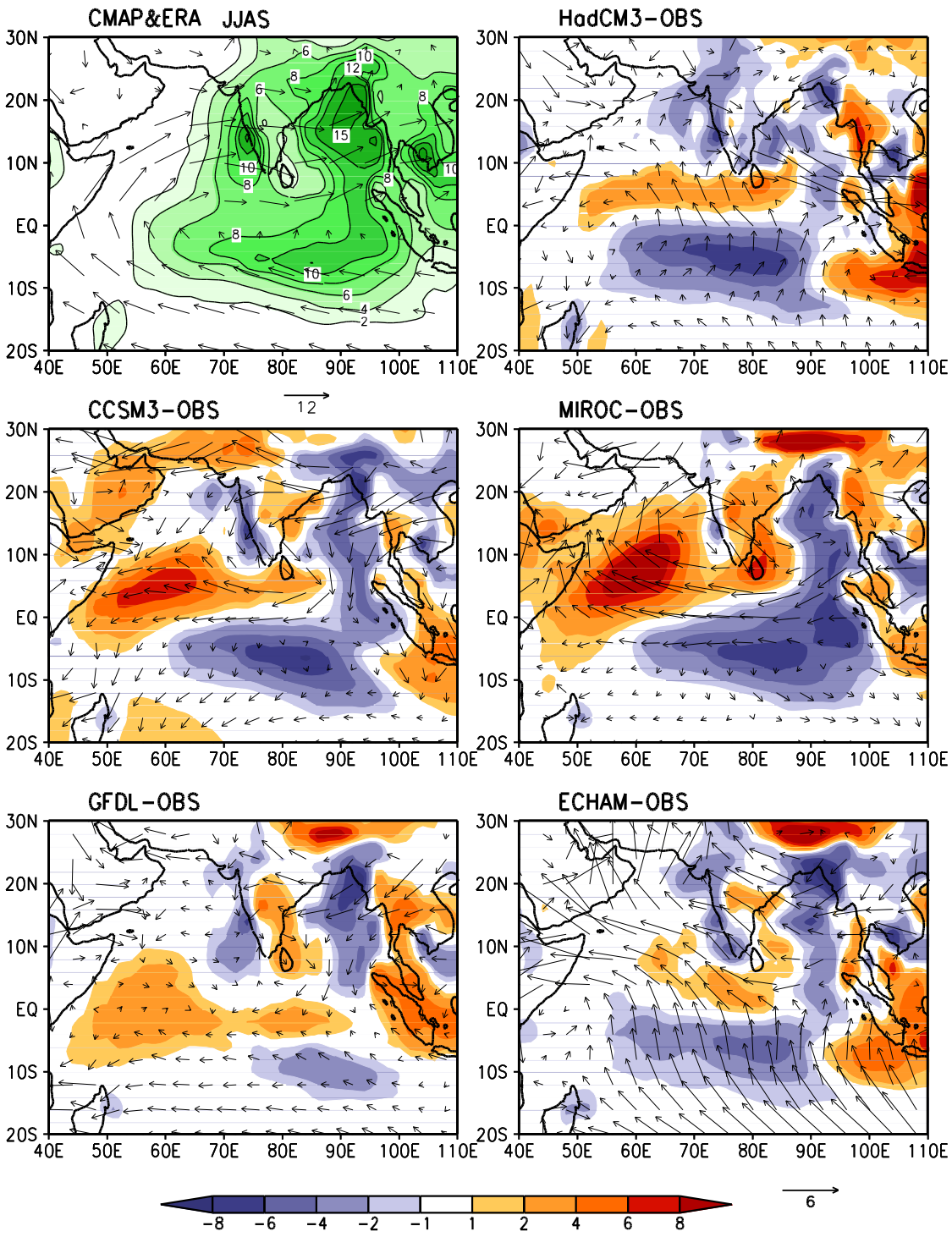

Figure 1: Seasonal mean (Jun-Sep; JJAS) precipitation (mm day^{-1}) and 850-hPa winds (m s^{-1}) for observations (top left) and differences model-observations (other panels).

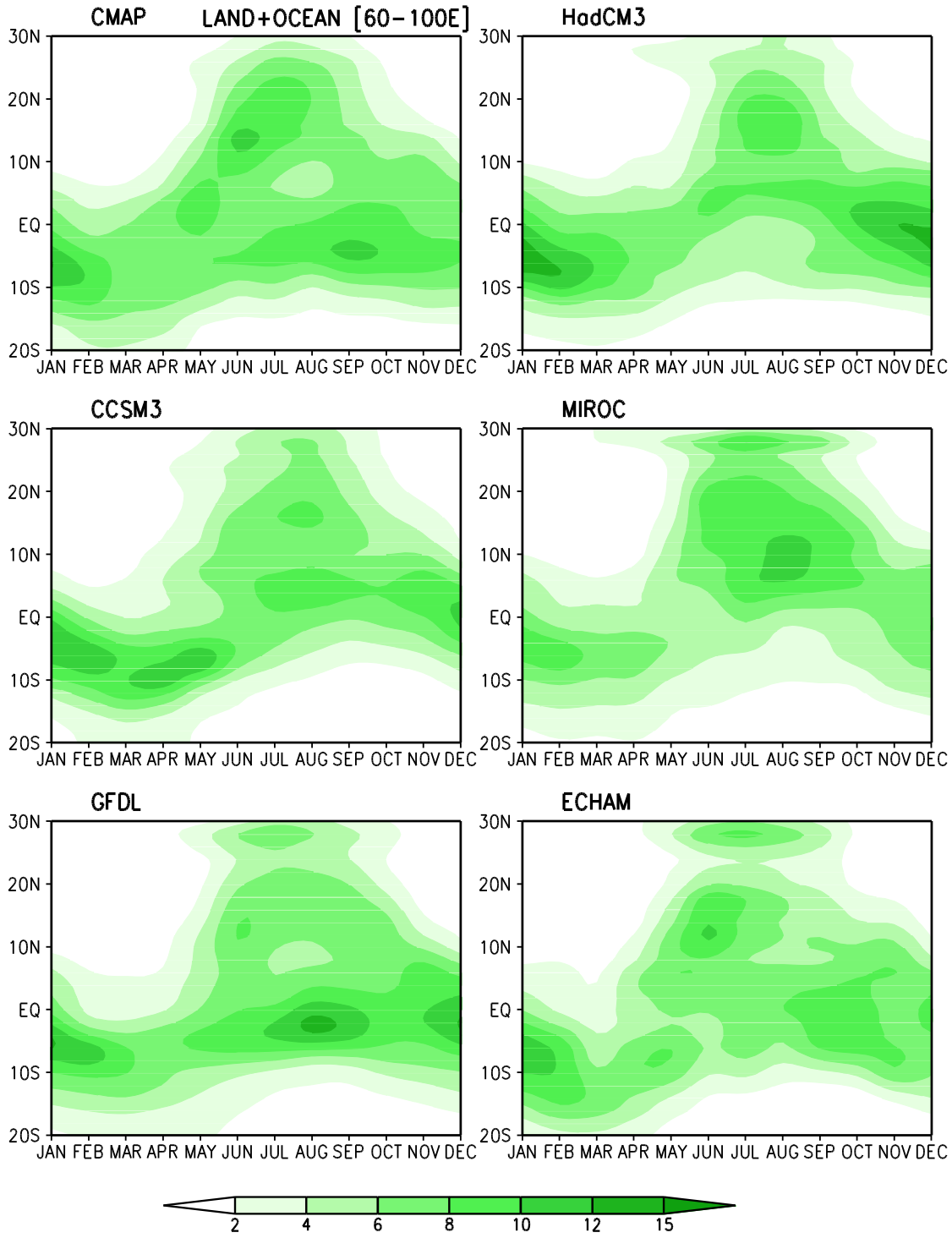

Figure 2: Time-latitude evolution of precipitation (mm day^{-1}) averaged over (60°-100°E; land and ocean points) for observations (top left) and coupled models (other panels).

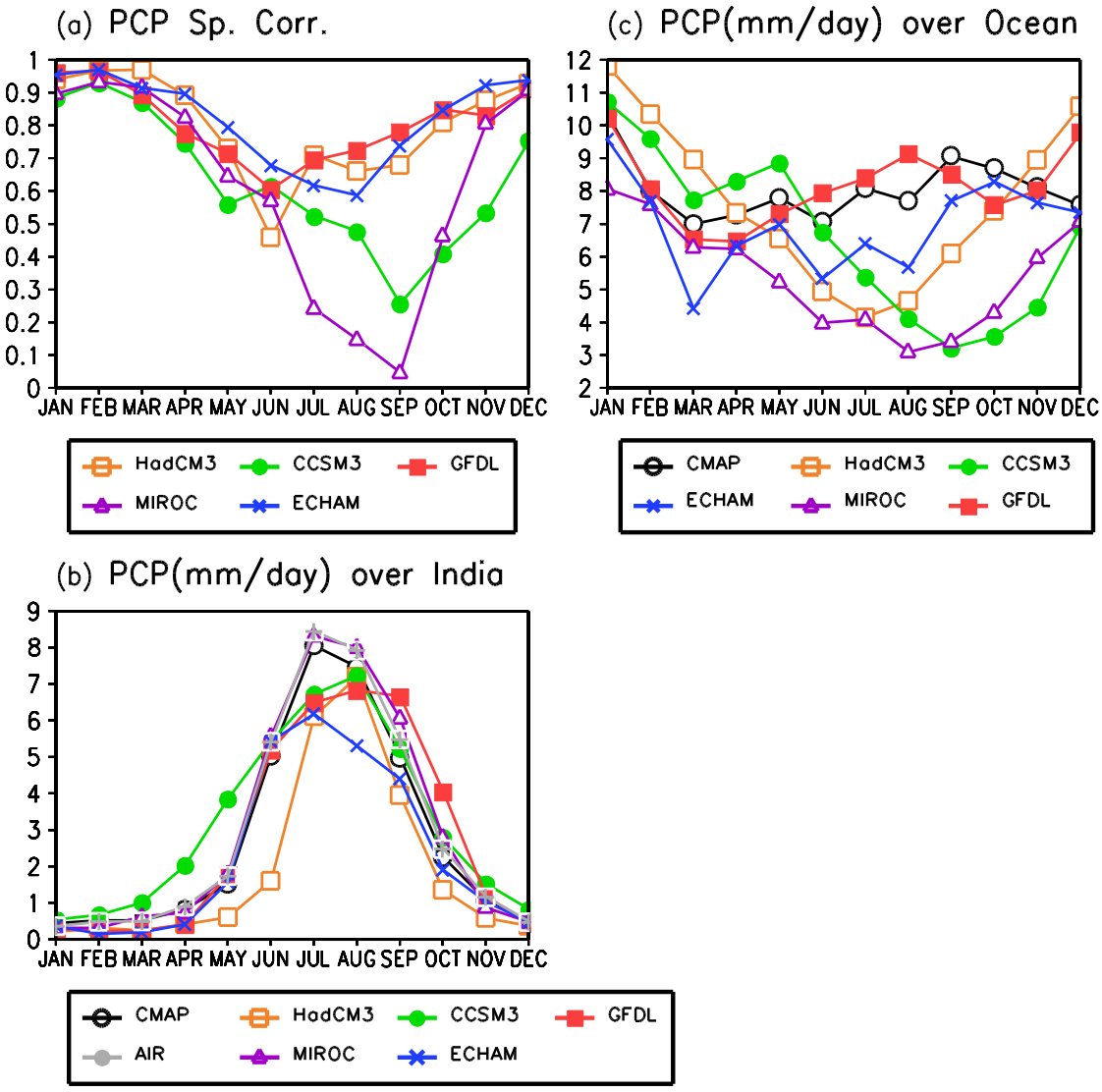

Figure 3: Annual cycle of (a) spatial correlation of model precipitation (averaged over 60°-100°E; 10°S-30°N; land and ocean points) with respect to CMAP, (b) observed and simulated precipitation (mm day^{-1}) averaged over India (land-only points), (c) observed and simulated precipitation (mm day^{-1}) averaged over (60°-100°E; 10°S-Equator) (ocean-only points).

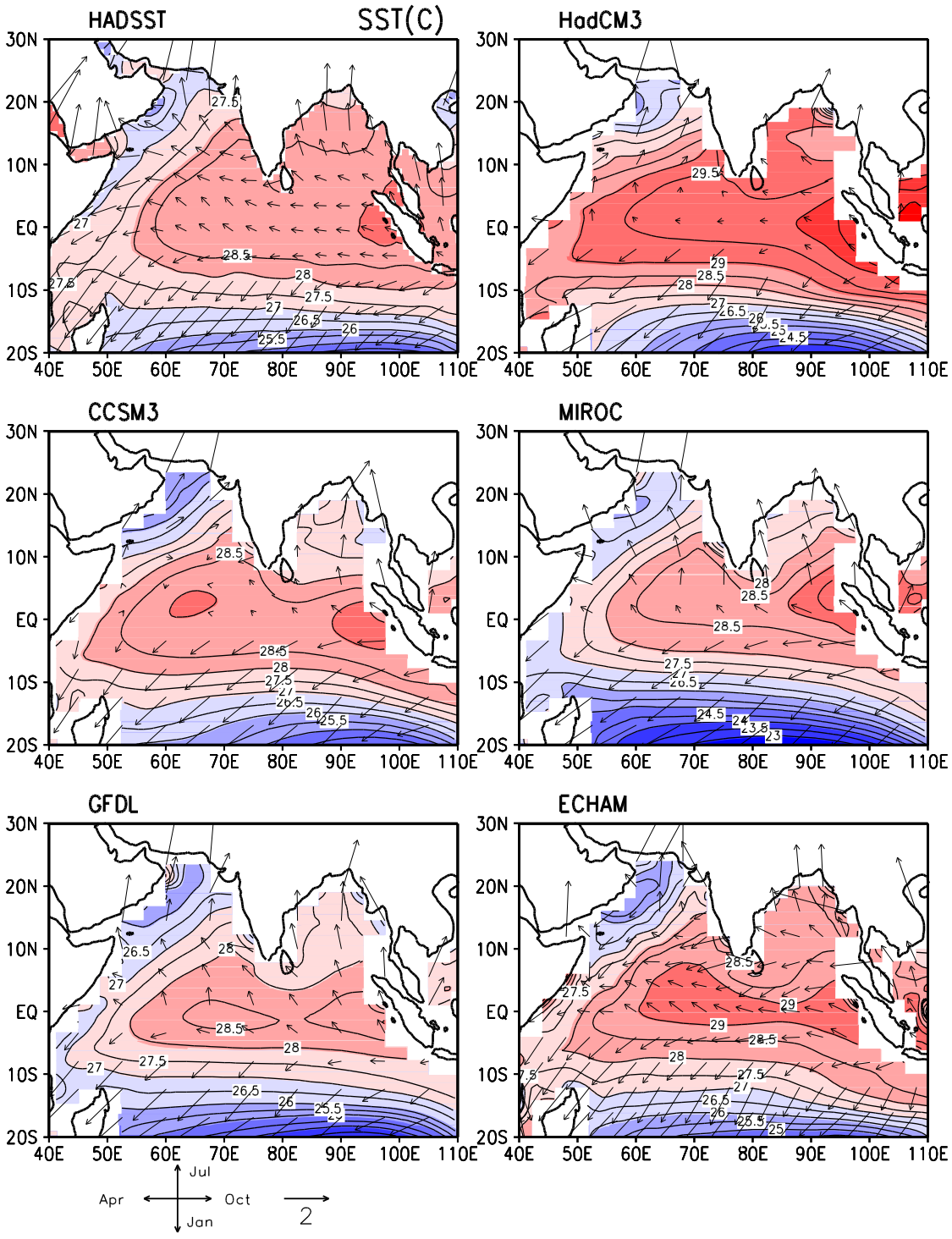

Figure 4: Annual mean SST (ºC, shaded) and amplitude and phase (arrows) of the annual cycle of SST over the Indian Ocean for observations (top left) and coupled models (other panels).

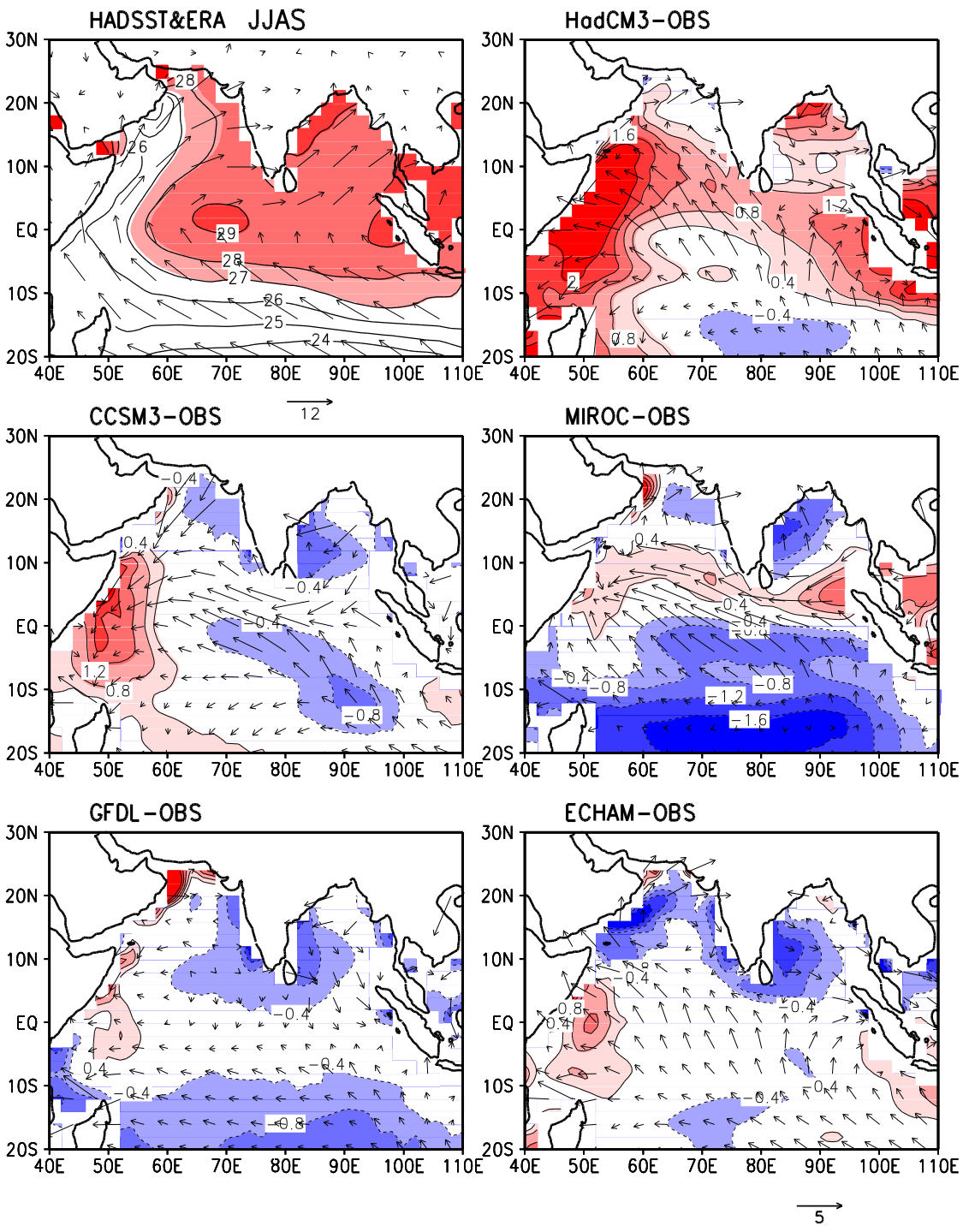

Figure 5: Seasonal mean (Jun-Sep; JJAS) SST (°C) and 1000-hPa winds (m s^{-1}) over the Indian Ocean for observations (top left) and differences model-observations (other panels).

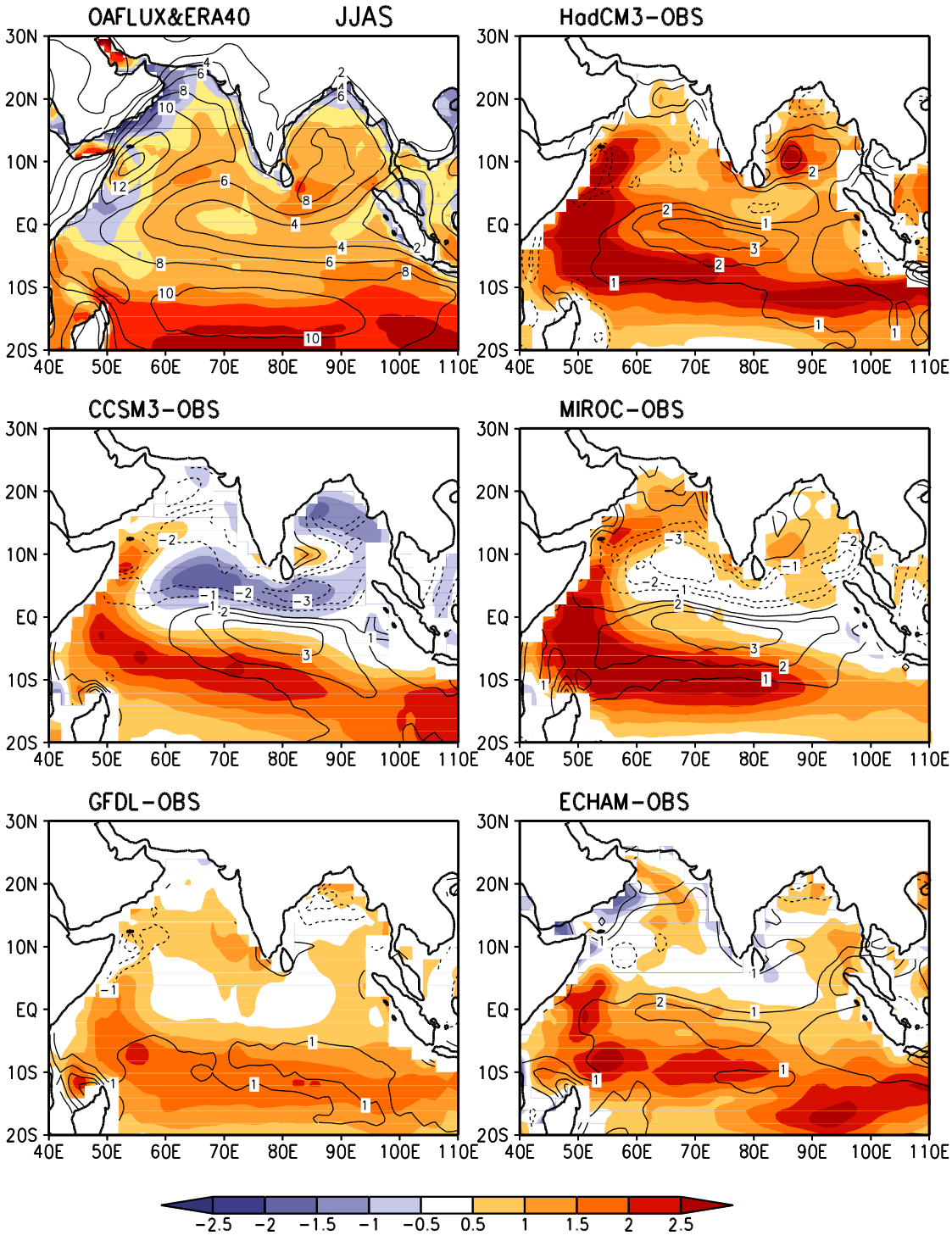

Figure 6: Seasonal mean (Jun-Sep; JJAS) evaporation (mm day^{-1}, shaded) and 1000-hPa wind speed (m s^{-1}, contours) over the Indian Ocean for observations (top left) and differences model-observations (other panels).

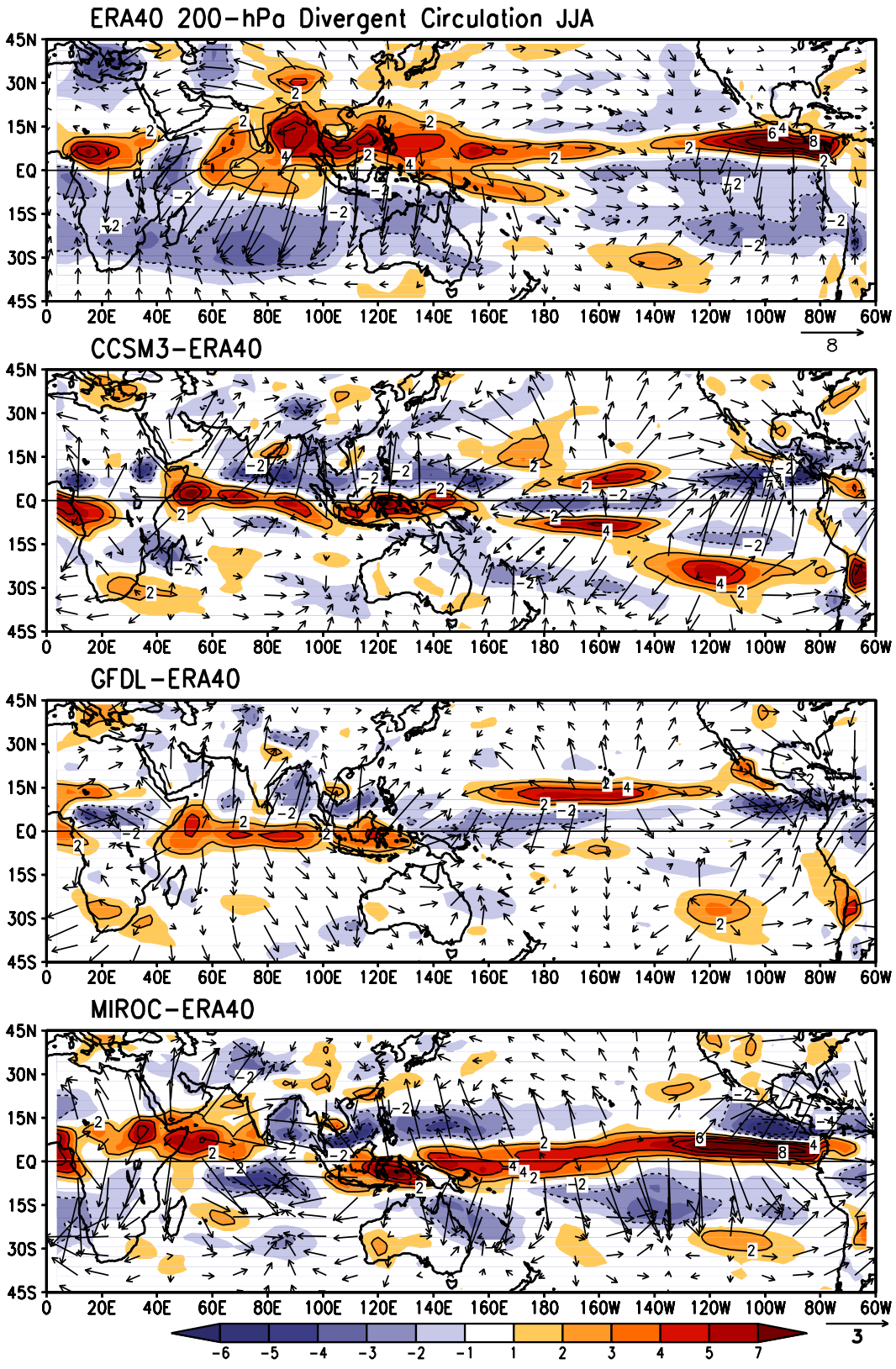

Figure 7: June-August mean (JJA) divergent wind (arrows) and divergence (10^{-6} s^{-1}; shaded) at 200 hPa in ERA40 (top) and differences model-ERA40 (other panels).

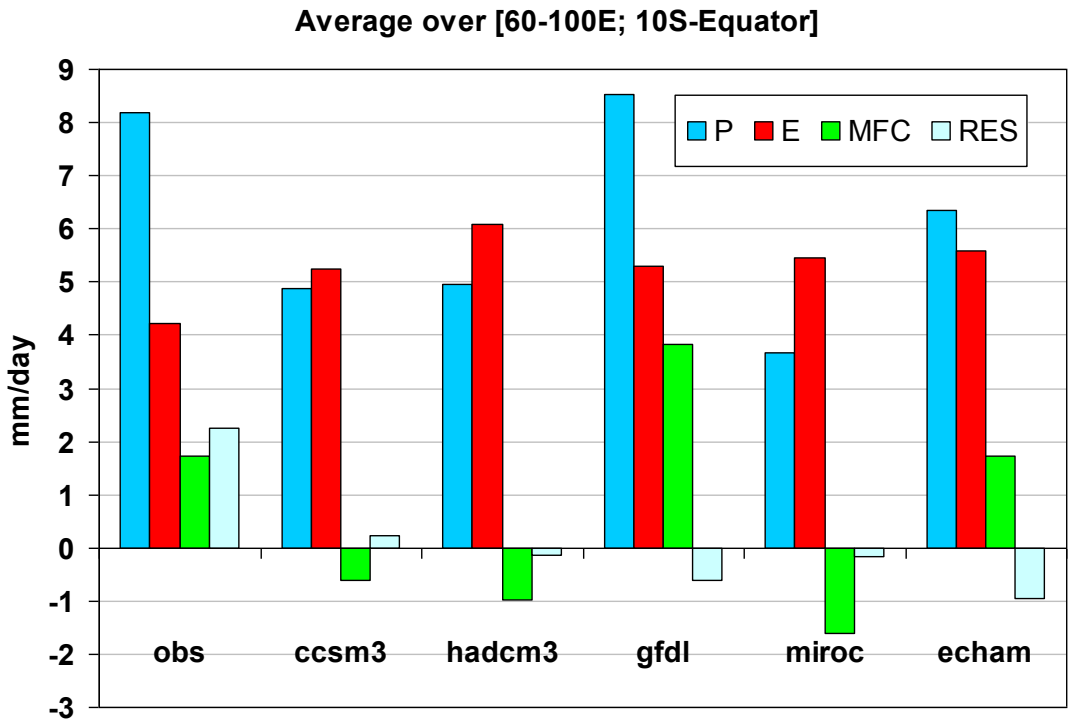

Figure 8: Seasonal (Jun-Sep) mean atmospheric water budget (in mm day^{-1}; P = precipitation; E = evaporation; MFC = vertically-integrated moisture flux convergence) averaged over (60°-100°E, 10°S-Equator).

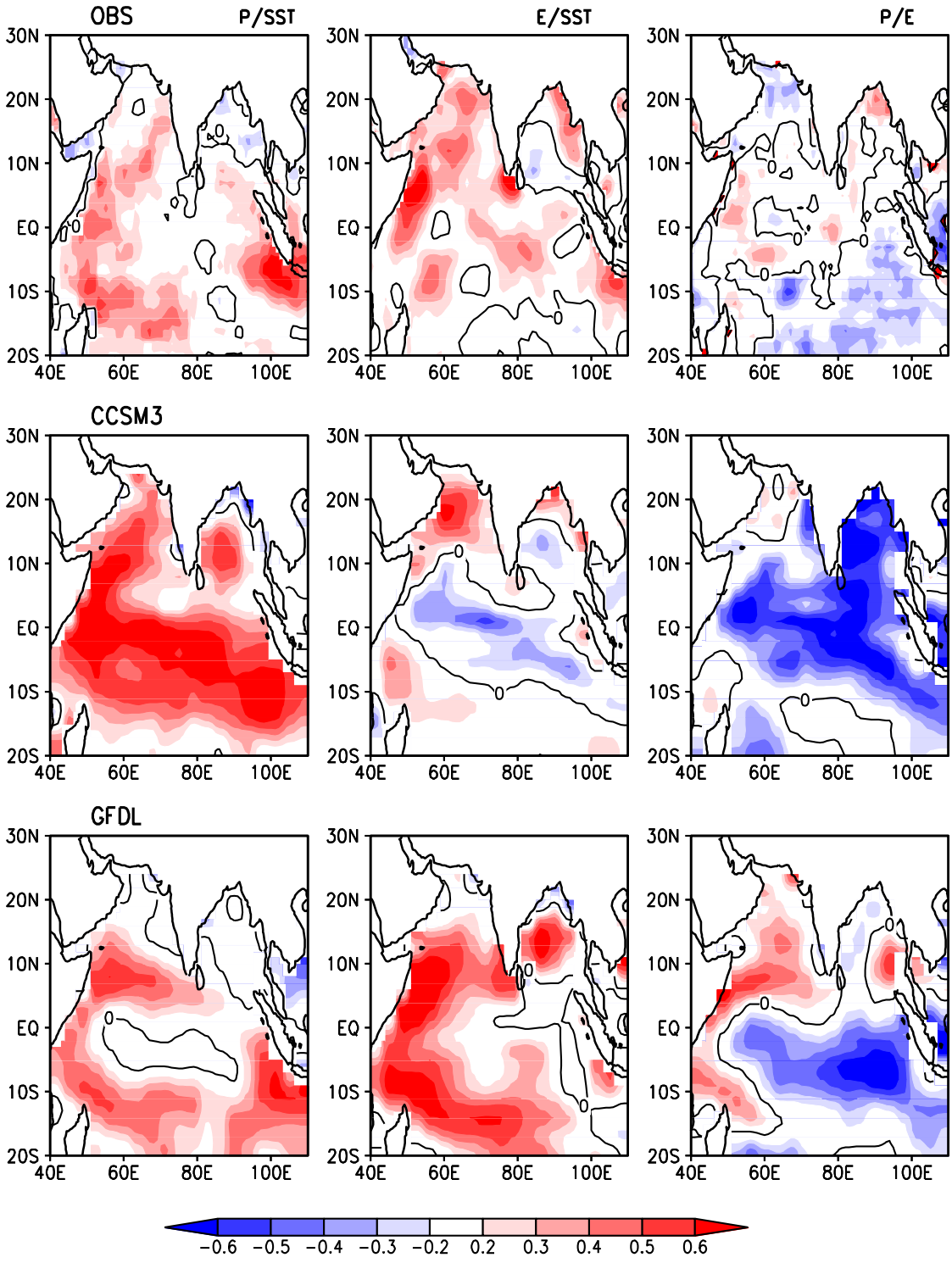

Figure 9a: June-August average pointwise and simultaneous correlations between precipitation and SST (left column), evaporation and SST (middle column), and precipitation and evaporation (right column) for observations (top), CCSM3 (middle), and GFDL (bottom). The zero-correlation contour is also displayed.

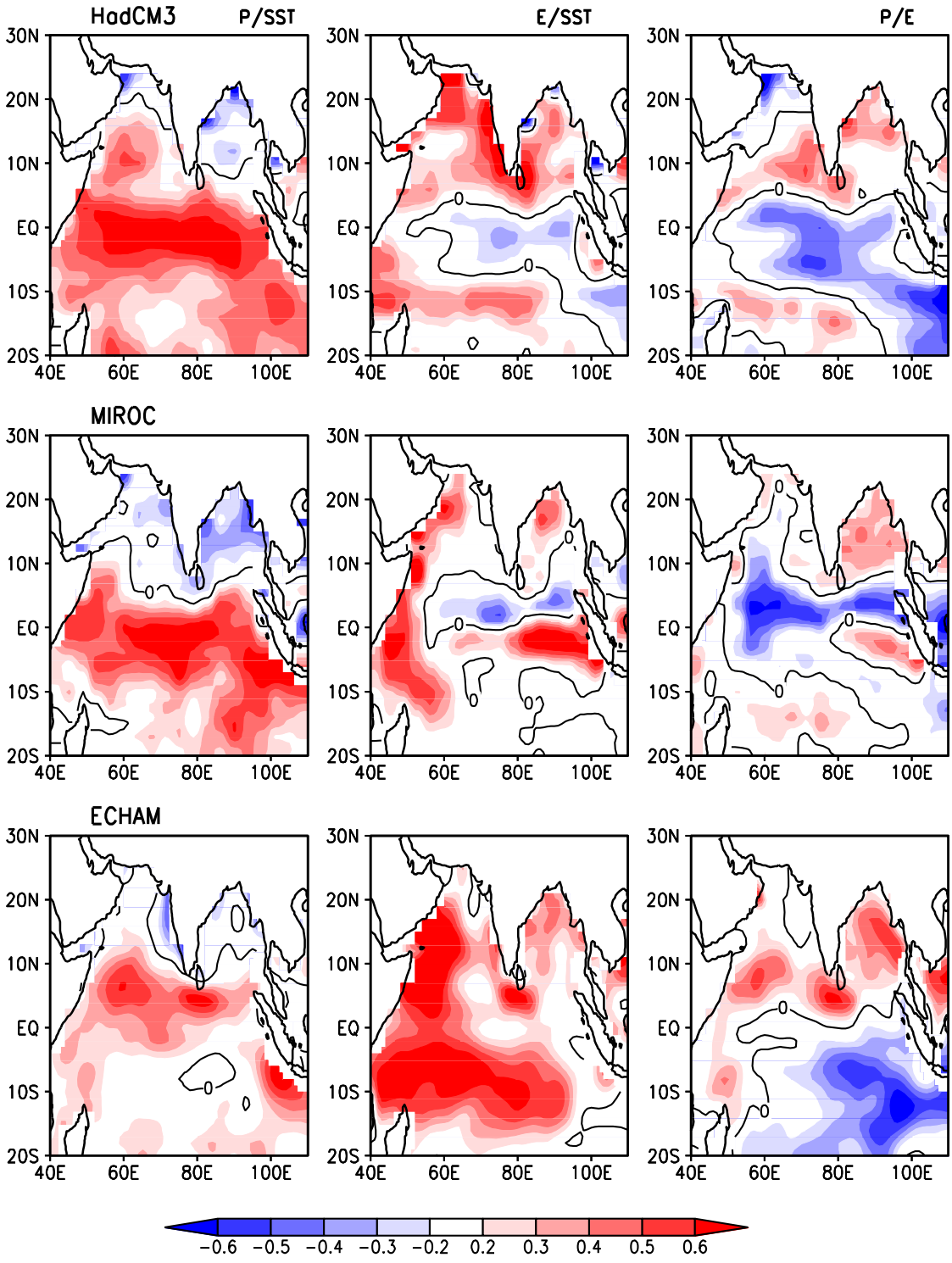

Figure 9b: The same as Fig. 9a, except for HadCM3 (top), MIROC (middle), and ECHAM (bottom).

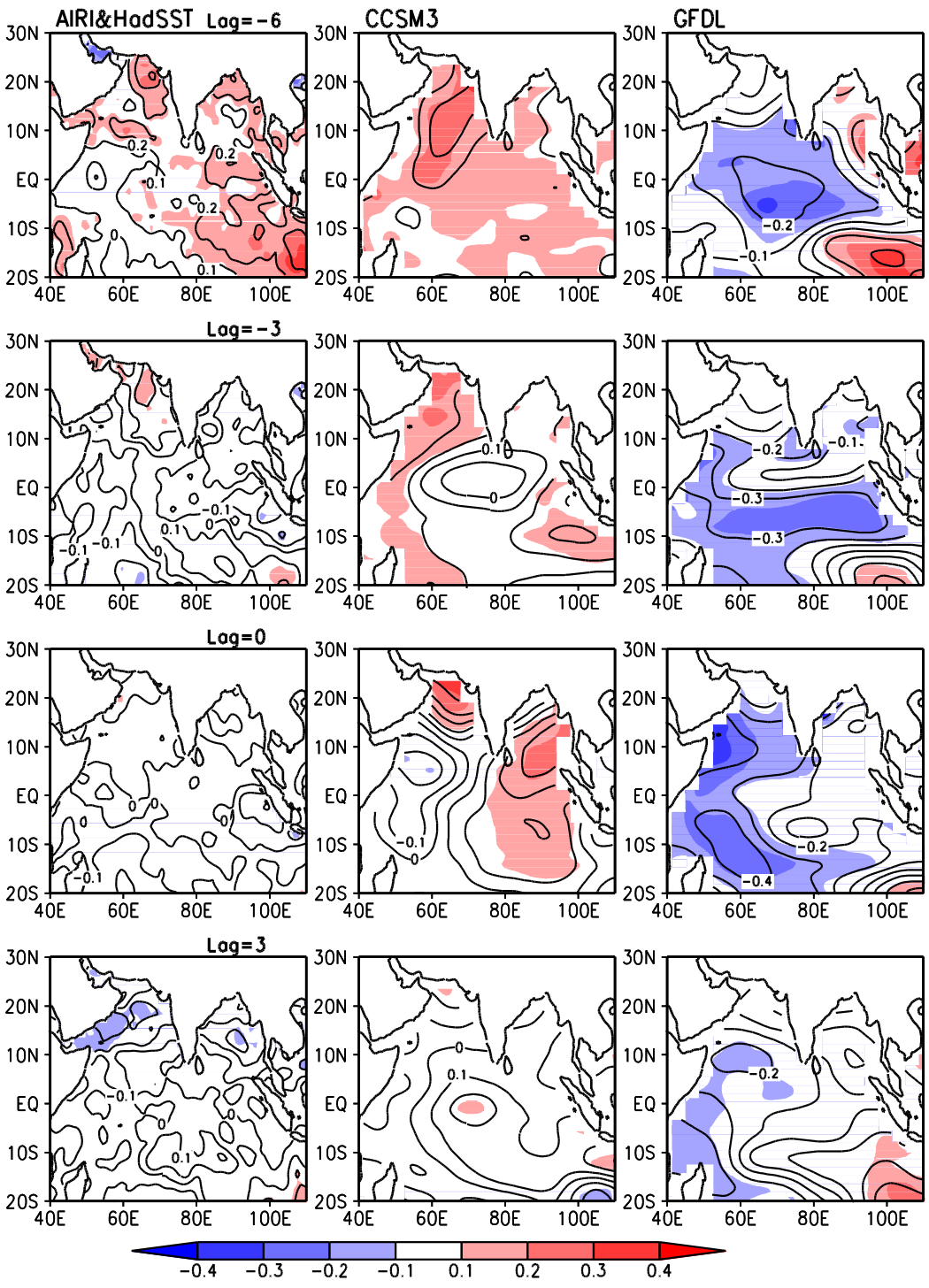

Figure 10a: Correlations (contour lines) and regressions (ºC; shaded) between Jun-Aug (JJA) precipitation over India and surrounding SST at (from top to bottom) lag -6, -3, 0, and +3 months (that is, SST of the previous DJF, MAM, contemporaneous JJA, and following SON, respectively) for observations (left), CCSM3 (middle), and GFDL (right).

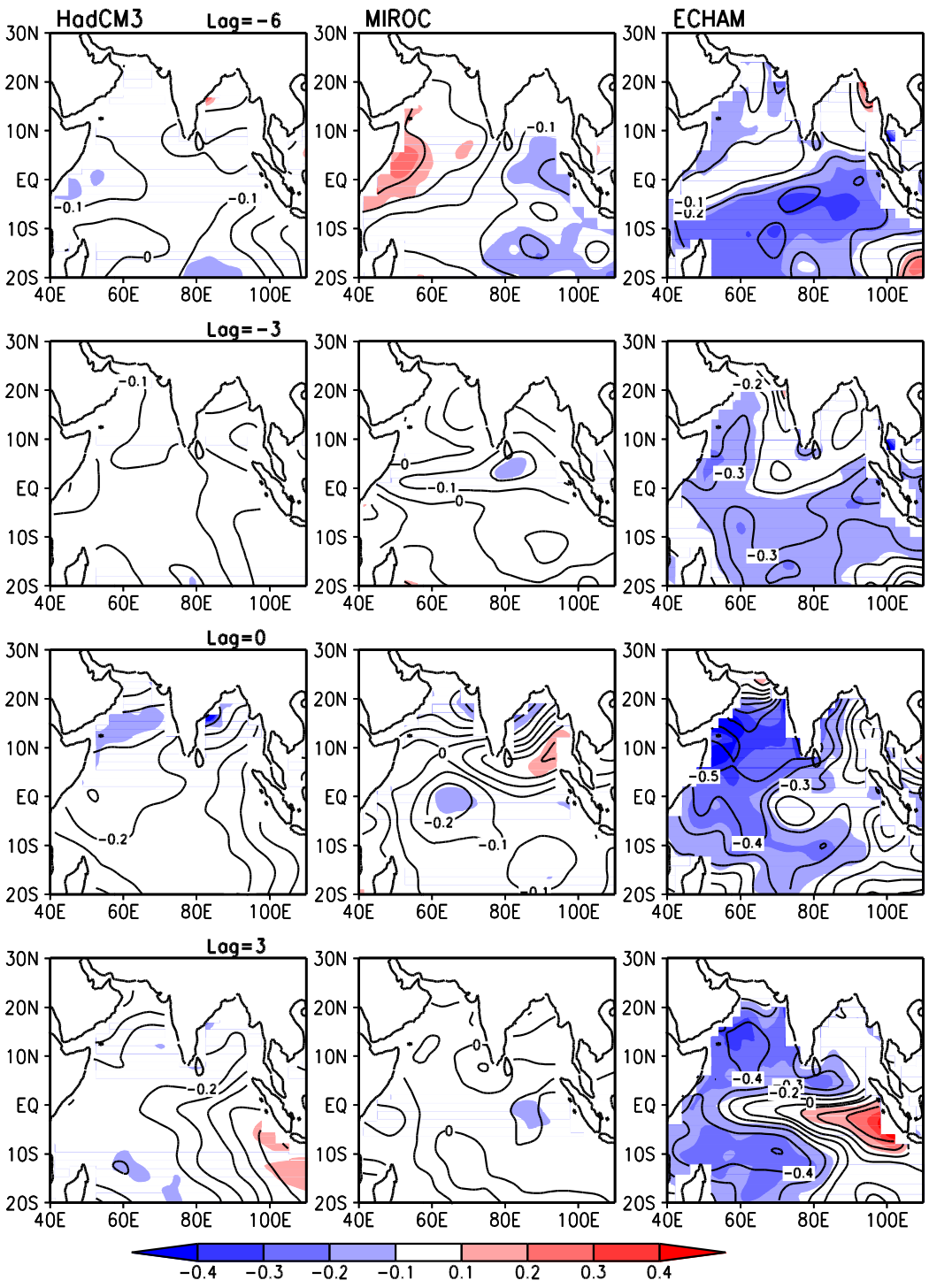

Figure 10b: The same as Fig. 10a, except for HadCM3 (left), MIROC (middle), and ECHAM (right).